



AFRL-RQ-WP-TP-2015-0148

**FREESTREAM EFFECTS ON BOUNDARY LAYER
DISTURBANCES FOR HIFIRE-5 (POSTPRINT)**

Matthew P. Borg and Roger L. Kimmel

**Hypersonic Sciences Branch
High Speed Systems Division**

Jerrod W. Hofferth and Rodney D.W. Bowersox

Texas A&M University

Chi L.N. Mai

**Air Force Materiel Command
96th Test Wing**

JANUARY 2015

Approved for public release; distribution unlimited.

See additional restrictions described on inside pages

STINFO COPY

**AIR FORCE RESEARCH LABORATORY
AEROSPACE SYSTEMS DIRECTORATE
WRIGHT-PATTERSON AIR FORCE BASE, OH 45433-7541
AIR FORCE MATERIEL COMMAND
UNITED STATES AIR FORCE**

NOTICE AND SIGNATURE PAGE

Using Government drawings, specifications, or other data included in this document for any purpose other than Government procurement does not in any way obligate the U.S. Government. The fact that the Government formulated or supplied the drawings, specifications, or other data does not license the holder or any other person or corporation; or convey any rights or permission to manufacture, use, or sell any patented invention that may relate to them.

This report was cleared for public release by the USAF 88th Air Base Wing (88 ABW) Public Affairs Office (PAO) and is available to the general public, including foreign nationals.

Copies may be obtained from the Defense Technical Information Center (DTIC)
(<http://www.dtic.mil>).

AFRL-RQ-WP-TP-2015-0148 HAS BEEN REVIEWED AND IS APPROVED FOR PUBLICATION IN ACCORDANCE WITH ASSIGNED DISTRIBUTION STATEMENT.

//Signature//

ROGER L. KIMMEL
Project Manager
Hypersonic Sciences Branch
High Speed Systems Division

//Signature//

MICHAEL S. BROWN, Chief
Hypersonic Sciences Branch
High Speed Systems Division
Aerospace Systems Directorate

//Signature//

THOMAS A. JACKSON
Deputy for Science
High Speed Systems Division
Aerospace Systems Directorate

This report is published in the interest of scientific and technical information exchange, and its publication does not constitute the Government's approval or disapproval of its ideas or findings.

Disseminated copies will show "//Signature//*" stamped or typed above the signature blocks.

REPORT DOCUMENTATION PAGE				<i>Form Approved</i> OMB No. 0704-0188	
<p>The public reporting burden for this collection of information is estimated to average 1 hour per response, including the time for reviewing instructions, searching existing data sources, gathering and maintaining the data needed, and completing and reviewing the collection of information. Send comments regarding this burden estimate or any other aspect of this collection of information, including suggestions for reducing this burden, to Department of Defense, Washington Headquarters Services, Directorate for Information Operations and Reports (0704-0188), 1215 Jefferson Davis Highway, Suite 1204, Arlington, VA 22202-4302. Respondents should be aware that notwithstanding any other provision of law, no person shall be subject to any penalty for failing to comply with a collection of information if it does not display a currently valid OMB control number. PLEASE DO NOT RETURN YOUR FORM TO THE ABOVE ADDRESS.</p>					
1. REPORT DATE (DD-MM-YY) January 2015		2. REPORT TYPE Conference Paper Postprint		3. DATES COVERED (From - To) 05 January 2014 – 05 January 2015	
4. TITLE AND SUBTITLE FREESTREAM EFFECTS ON BOUNDARY LAYER DISTURBANCES FOR HIFIRE-5 (POSTPRINT)				5a. CONTRACT NUMBER In-house	
				5b. GRANT NUMBER	
				5c. PROGRAM ELEMENT NUMBER 61102F	
6. AUTHOR(S) Matthew P. Borg and Roger L. Kimmel (AFRL/RQHF) Jerrod W. Hofferth and Rodney D.W. Bowersox (Texas A&M University) Chi L.N. Mai (AFMC 96)				5d. PROJECT NUMBER 3002	
				5e. TASK NUMBER N/A	
				5f. WORK UNIT NUMBER Q1FN	
7. PERFORMING ORGANIZATION NAME(S) AND ADDRESS(ES) Hypersonic Sciences Branch (AFRL/RQHF) High Speed Systems Division Air Force Research Laboratory, Aerospace Systems Directorate Wright-Patterson Air Force Base, OH 45433-7541 Air Force Materiel Command, United States Air Force				8. PERFORMING ORGANIZATION REPORT NUMBER AFRL-RQ-WP-TP-2015-0148	
9. SPONSORING/MONITORING AGENCY NAME(S) AND ADDRESS(ES) Air Force Research Laboratory Aerospace Systems Directorate Wright-Patterson Air Force Base, OH 45433-7541 Air Force Materiel Command United States Air Force				10. SPONSORING/MONITORING AGENCY ACRONYM(S) AFRL/RQHF	
				11. SPONSORING/MONITORING AGENCY REPORT NUMBER(S) AFRL-RQ-WP-TP-2015-0148	
12. DISTRIBUTION/AVAILABILITY STATEMENT Approved for public release; distribution unlimited.					
13. SUPPLEMENTARY NOTES PA Case Number: 88ABW-2014-5544; Clearance Date: 01 Dec 2014. This conference paper was published in the proceedings of the 53rd AIAA Aerospace Sciences Meeting (AIAA) Conference, held January 5 - 9, 2015 in Kissimmee, FL. The U.S. Government is joint author of the work and has the right to use, modify, reproduce, release, perform, display, or disclose the work. This is a work of the U.S. Government and is not subject to copyright protection in the United States.					
14. ABSTRACT A 2:1 elliptic cone model was tested in a variable-Mach-number conventional hypersonic wind tunnel. Freestream Reynolds number, Mach number, model streamwise location, and model wall temperature were all varied to ascertain the effect of each on measured disturbances. A low-frequency disturbance was observed at Mach 5.8. It experienced some growth in excess of the increasing freestream pressure and noise for a narrow Reynolds number range. Disturbance properties were similar to what was measured in another conventional hypersonic wind tunnel. For Mach 6.5 and 7, there was no evidence of traveling crossflow waves. However, higher-frequency disturbances were observed. These disturbances were nearly two-dimensional and had phase speeds near the expected edge velocity. It is possible that these disturbances were second mode waves. None of the measured disturbances corresponded to any feature of the freestream Pitot spectra.					
15. SUBJECT TERMS boundary layer transition, hypersonic, ground test					
16. SECURITY CLASSIFICATION OF:			17. LIMITATION OF ABSTRACT: SAR	18. NUMBER OF PAGES 27	19a. NAME OF RESPONSIBLE PERSON (Monitor) Roger L. Kimmel 19b. TELEPHONE NUMBER (Include Area Code) N/A
a. REPORT Unclassified	b. ABSTRACT Unclassified	c. THIS PAGE Unclassified			

Freestream Effects on Boundary Layer Disturbances for HIFiRE-5

Matthew P. Borg,^{*} Roger L. Kimmel[†]

Air Force Research Laboratory, Aerospace Systems Directorate, WPAFB, OH 45433-7542

Jerrold W. Hofferth,[‡] Rodney D. W. Bowersox[§]

Texas A&M University, College Station, Texas 77843-3141

Chi L. N. Mai[¶]

United States Air Force, Eglin AFB, FL 32542

Abstract

A 2:1 elliptic cone model was tested in a variable-Mach-number conventional hypersonic wind tunnel. Freestream Reynolds number, Mach number, model streamwise location, and model wall temperature were all varied to ascertain the effect of each on measured disturbances. A low-frequency disturbance was observed at Mach 5.8. It experienced some growth in excess of the increasing freestream pressure and noise for a narrow Reynolds number range. Disturbance properties were similar to what was measured in another conventional hypersonic wind tunnel. For Mach 6.5 and 7, there was no evidence of traveling crossflow waves. However, higher-frequency disturbances were observed. These disturbances were nearly two-dimensional and had phase speeds near the expected edge velocity. It is possible that these disturbances were second mode waves. None of the measured disturbances corresponded to any feature of the freestream Pitot spectra.

I. Introduction

The Hypersonic International Flight Research Experimentation (HIFiRE) program is a hypersonic flight test program jointly executed by the Air Force Research Laboratory (AFRL) and the Australian Defence Science and Technology Organization (DSTO).^{1,2} The purpose of this research is to develop and validate technologies critical to the development of next generation hypersonic aerospace systems. HIFiRE-5 is the second of two flights in the HIFiRE manifest focused on boundary-layer transition. The HIFiRE-5 flight is devoted to measuring transition on a three-dimensional (3D) body.

Extended hypersonic flight with lifting configurations requires improved understanding and prediction of 3D transition. Transition on 3D configurations embodies several phenomena not encountered on axisymmetric configurations at zero degree angle-of-attack, including swept leading-edge or attachment-line transition and crossflow instabilities (including crossflow interactions with other instability mechanisms shared with axisymmetric flow configurations such as first and second mode instabilities). Very limited hypersonic flight data exist for any of these phenomena.³ The need for a better understanding of 3D transition motivates the HIFiRE-5 flight and ground-test experiments.

The crossflow instability can become the dominant path to boundary layer transition for realistic, 3D vehicle configurations. Both stationary and traveling modes are possible. The stationary mode manifests as co-rotating, streamwise vortices, while traveling crossflow wavefronts are inclined relative to the inviscid streamlines.³ The wave number vector of the most unstable traveling mode has a spanwise component oppo-

^{*}Research Aerospace Engineer, Senior Member AIAA

[†]Senior Research Engineer, Associate Fellow AIAA

[‡]Postdoctoral Researcher, Member AIAA

[§]Professor, Aerospace Engineering, Associate Fellow AIAA

[¶]Aerospace Engineer, Senior Member AIAA

This material has been cleared for public release. Case Number 88ABW-2014-5544.

Approved for public release; distribution unlimited.

1 of 24

American Institute of Aeronautics and Astronautics

site the direction of the crossflow.⁴ For incompressible flows, the stationary modes are typically dominant in low noise environments of flight and “quiet” wind tunnels; whereas the traveling modes tend to dominate in conventional tunnels.⁵ The stationary mode is thought to be seeded by surface roughness, while the traveling mode is generated by vortical disturbances in the freestream which are entrained in the boundary layer.⁶

Considerable study has been made of crossflow instabilities for incompressible flows.^{5–11} It has been established that stationary modes undergo a period of linear growth, saturate nonlinearly, and then develop secondary instabilities that rapidly lead to transition.^{5,9} The majority of historic crossflow research has focused on stationary modes, since this is expected to be the dominant crossflow instability in the low-noise flight environment. However, the role and importance of traveling modes, possible interactions with stationary crossflow, and possible nonlinear self-interaction have not been well documented.

Likewise, relatively little crossflow research has focused on supersonic or hypersonic flows. Saric^{5,12} suggested that the same basic behavior observed for incompressible flows should also be expected for compressible flows. King¹³ measured crossflow-dominated transition on a 5 degree sharp circular cone at Mach 3.5 in both quiet and noisy flow. However, these experiments focused primarily on crossflow transition location rather than a detailed study of the instabilities themselves. He noted that the effect of freestream turbulence on transition location decreased substantially with increasing crossflow. Recent experiments by Beeler et al.¹⁴ confirmed the presence of stationary crossflow vortices on a wedge-cone model in a Mach 3.5 quiet tunnel. Future experiments will focus on determining if traveling modes are also present. Poggie and Kimmel¹⁵ measured traveling crossflow wave properties with hot films in a Mach 8 conventional tunnel using a 2:1 elliptic cone, but did not find good agreement with complementary computations. They suggested that the poor agreement was due to the limitations of the computations. Malik et al.³ reported experimental and computational results from a crossflow-dominated supersonic swept-wing flight test for Mach numbers from four to five. The flight transition locations correlated with stationary crossflow N-factors of 7.0–12.4 and traveling crossflow N-factors of 7.6–14.1. Choudhari et al.¹⁶ described stability computations for flight and wind tunnel conditions for HIFiRE-5. They found strong stationary and traveling crossflow growth over large portions of the vehicle acreage. They also investigated the effect of flow non-parallelism and integration path on N-factors for both types of crossflow instability. Swanson and Schneider¹⁷ detected stationary crossflow vortices with temperature sensitive paint at Mach 6 with both quiet and conventional freestream noise levels. Reference 18 describes previous experiments for the HIFiRE-5 geometry that primarily focused on stationary crossflow modes in Purdue’s Boeing/AFOSR Mach-6 Quiet Tunnel (BAM6QT). Surface pressure measurements and oil flow visualization clearly showed that both stationary and traveling crossflow modes coexist in a very low-noise, flight-like environment. Additional experiments, described in Reference 19, focused on the traveling crossflow instability. Using pressure sensors mounted flush with the model surface, traveling crossflow wave angles and phase speeds were measured in quiet flow and found to be in good agreement with computations. For noisy flow, the model boundary layer was observed to transition, but no instability waves were measured.

II. Experimental Overview

In an attempt to study traveling crossflow waves in both conventional “noisy” and quiet freestream environments, previous experiments were performed on the HIFiRE-5 elliptic cone geometry in Purdue University’s BAM6QT.^{18,19} The results of these experiments motivate the current work. Traveling crossflow waves and transition were clearly measured in the quiet freestream environment. Since the traveling mode is conventionally thought to dominate crossflow transition in noisy environments, traveling waves were also expected in noisy flow. However, there was no evidence of traveling crossflow waves with a noisy freestream, even though the spectra of the surface pressure signals showed an expected progression from laminar to turbulent as the Reynolds number was increased. It was thought that perhaps the very noisy freestream environment of the BAM6QT when run noisy caused transition apart from the traveling crossflow mode. It was thus desired to duplicate the Mach number, freestream Reynolds numbers, and total temperature in another conventional wind tunnel with lower freestream noise to see if traveling waves would be present.

The Actively Controlled Expansion (ACE) tunnel at Texas A&M University was used for the experiments reported here. The ACE has a two-dimensional contoured nozzle capable of continuous Mach numbers ranging from 5–7. The Mach number is altered by changing the throat area between runs.

For the present experiments, freestream unit Reynolds numbers ranging from about $0.8\text{--}6.5 \times 10^6/\text{m}$ were realized. The tunnel operated for approximately 40 s per run. The stagnation pressure was easily changed

throughout the run. Two tunnel runs were generally needed to complete an entire Reynolds number sweep. The tunnel operator typically started the tunnel at a pressure near the midpoint of the pressure range. He would then decrease or increase the stagnation pressure in steps of about 35 kPa, keeping the pressure constant for around 1 s at each step. In this manner, many periods of steady Reynolds number flow were obtained during each run.

Prior to the run, hot air was passed through the tunnel in order to bring the piping up to the desired stagnation temperature. Without this provision, the flow would lose considerable heat during the experiments and would not be at the desired stagnation temperature. For most of the present work, the model was left outside of the tunnel during this pre-heat period, and was quickly installed in the tunnel between the pre-heat and the tunnel run. Thus, the model was approximately 295 K at the beginning of each run. There were two runs for which an elevated model temperature were desired. This was accomplished by leaving the model in the tunnel during the preheat. This step resulted in a model wall temperature of approximately 332 K. The stagnation temperature was approximately 430 K for Mach 5.8, and approximately 460 K for Mach 6.5 and 7. The ACE facility is described in greater detail in References 20–22.

The experimental results presented in this paper were obtained with the model at 0.0 degrees angle-of-attack and yaw. The uncertainty in angle of attack was estimated to be 0.1 degrees. Since it was expected that the freestream noise conditions could change with position in the tunnel, the model was located at one of three streamwise stations. The baseline station, referred to as MID, positioned the nosetip about 84 mm upstream of the nozzle exit plane. The upstream position, US, moved the model approximately 193 mm farther upstream, with most of the model in the nozzle. Previous computations of the nozzle flow revealed that the nosetip would still be downstream of the most downstream nozzle characteristic. A final downstream station, DS, positioned the model about 152 mm downstream of the MID station. Relative to the nozzle exit plane, this put the model nosetip 277, 84, and -68 mm from the nozzle exit plane for the US, MID, and DS stations, respectively (here, positive numbers indicate a position upstream of the nozzle exit plane). Table 1 shows the combinations of Mach number and streamwise station that were tested in these experiments. The US station was also tested at Mach 6, but freestream measurements there revealed problems with the flow quality. Thus these data are not presented.

Table 1: Condition matrix

Mach/Location	US	MID	DS
5.8		•	•
6.5	•		
7	•	•	

Kulite XCQ-062-15A and XCE-062-15A pressure transducers with A screens were mounted flush with the model surface to detect traveling crossflow waves. The Kulite sensors are mechanically stopped at about 100 kPa so that they can survive exposure to high pressures but still maintain the sensitivity of a 100 kPa full-scale sensor. These sensors typically have flat frequency response up to about 30–40% of their roughly 270–285 kHz resonant frequency.²³ The pressure sensors were anti-alias filtered at 200 kHz using 8-pole Bessel filters. The model temperature was measured with a Medtherm Type T thermocouple mounted flush with the surface of the model at the same location as one of the Kulite sensors, but reflected over the model centerline.

For the current experiments, five pressure sensors were used. Table 2 lists the locations of the sensors relative to the nosetip. Here, x and y are the streamwise and spanwise coordinates, respectively. Figure 1 shows a sketch of the aft end of the instrumented quadrant of the model and sensor locations. The sensors were located in a region of the model that had previously shown strong stationary crossflow vortices and large traveling crossflow N-factors.^{16, 18, 24, 25}

In order to more fully understand the model boundary layer's response to the freestream disturbance field, attendant freestream Pitot surveys were also completed on the tunnel centerline for all of these conditions and streamwise stations. The Pitot sensor was a Kulite XCEL-100-5A with a B screen and had a resonant frequency of about 140 kHz. The Pitot signal was anti-alias filtered at 100 kHz with an 8-pole Butterworth filter.

Table 2: Instrumentation locations and notation

Sensor	x (mm)	y (mm)
1	310.1	41.2
2	312.6	45.1
3	312.6	39.8
4	315.5	43.0
5	318.1	39.8

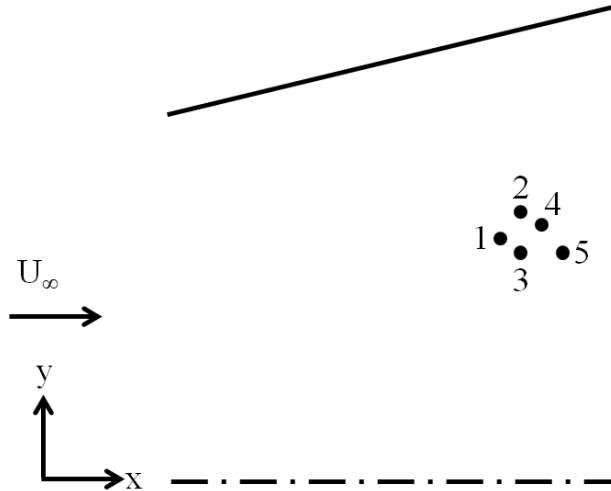


Figure 1: Schematic of pressure-sensor locations

II.A. Model Description

The elliptic cone configuration was chosen as the test-article geometry based on previous testing and analysis for elliptic cones.^{26–28} This prior work demonstrated that the 2:1 elliptic cone would generate significant crossflow instability at the expected flight conditions. In order to exploit this prior body of work and expedite configuration development, the 2:1 elliptical geometry was selected as the HIFiRE-5 test article.

The model, shown in Figure 2, is a 38.1% scale model of the flight vehicle. It is 328.1 mm long and has a base semimajor axis of 82.3 mm. The half-angle of the elliptic cone test article in the minor axis plane is 7.00° , and 13.80° in the major axis (x - y plane). The nose tip cross-section in the minor axis plane is a 0.95 mm radius circular arc, tangent to the cone ray describing the minor axis, and retains a 2:1 elliptical cross-section to the tip.

The 76.2-mm-long nosetip is fabricated from 15-5 stainless steel, followed by a frustum made of 7075T6 aluminum. For the present experiments, much of the model acreage was spray-painted black. The paint was left on the model after previous fluorescent oil flow visualization. The edges of the paint were sanded with fine-grit sand paper to smoothly transition the model surface from the bare aluminum finish to the paint layer. The pressure sensors were mounted flush with the paint. A more complete description of the model can be found in Reference 24.



Figure 2: Wind tunnel model, looking down on semi-major axis plane

II.B. Calculation of Disturbance Properties

The utilization of three sensors allows the calculation of disturbance phase speed and wave angle as a function of frequency using the cross spectrum, since two unique sensor pairs are needed. The following procedure was taken from References 15 and 29 and is used to calculate disturbance properties. The complex-valued cross spectrum of the signals from two sensors is given by:

$$S_{12}(f) = \lim_{T \rightarrow \infty} (1/T) E[\hat{s}_1^*(f, T) \hat{s}_2(f, T)] \quad (1)$$

where $\hat{s}(f)$ is the Fourier transform of a signal, E is the expected value operator, f is frequency, T is the record length, and $*$ denotes the complex conjugate. A real-valued method of measuring the amplitude of the cross spectrum is the coherence, given by:

$$\gamma^2(f) = \frac{|S_{12}(f)|^2}{S_{11}(f)S_{22}(f)} \quad (2)$$

The coherence is a frequency-dependent cross correlation of the signals with values ranging from 0 to 1. A value of 0 signifies no correlation between the two signals and a value of 1 means perfect correlation. The coherence gives a good idea of the frequency range over which the cross spectrum is meaningful. The phase spectrum can then be found by:

$$\phi(f) = \arctan \left(\frac{\Im[S_{12}]}{\Re[S_{12}]} \right) \quad (3)$$

where \Im and \Re represent the imaginary and real components, respectively. The time delay associated with the phase spectrum is given by:

$$\tau(f) = \phi(f)/2\pi f \quad (4)$$

Knowing the time delay for two sensor pairs and the relative locations of the sensors enables the calculation of disturbance wave angle and phase speed. Wave angles and phase speeds are shown below for various several disturbances.

III. Tunnel Freestream Characterization

The Mach number for every tunnel condition is determined by measuring the stagnation pressure in the settling chamber (P_{t1}) with an Endevco 8540-200 piezoresistive transducer used as a Pitot probe and the nozzle static pressure (P_1) near the nozzle exit plane with a temperature-stabilized 10-Torr MKS Baratron pressure transducer. Assuming isentropic flow through the nozzle, the Mach number is determined from these two pressures. The Mach number can also be determined using the measured freestream Pitot pressure, P_{t2} , and P_{t1} , and assuming a normal shock in front of the Pitot probe. The Mach number obtained from P_{t1} and

Approved for public release; distribution unlimited.

P_1 should match that obtained from P_{t1} and P_{t2} . Both methods of determining Mach number versus P_{t1} for all tunnel conditions and locations are shown in Figure 3. The open symbols represent the Mach number determined from P_{t1} and P_{t2} , while the close symbols are the Mach number determined from P_{t1} and P_1 .

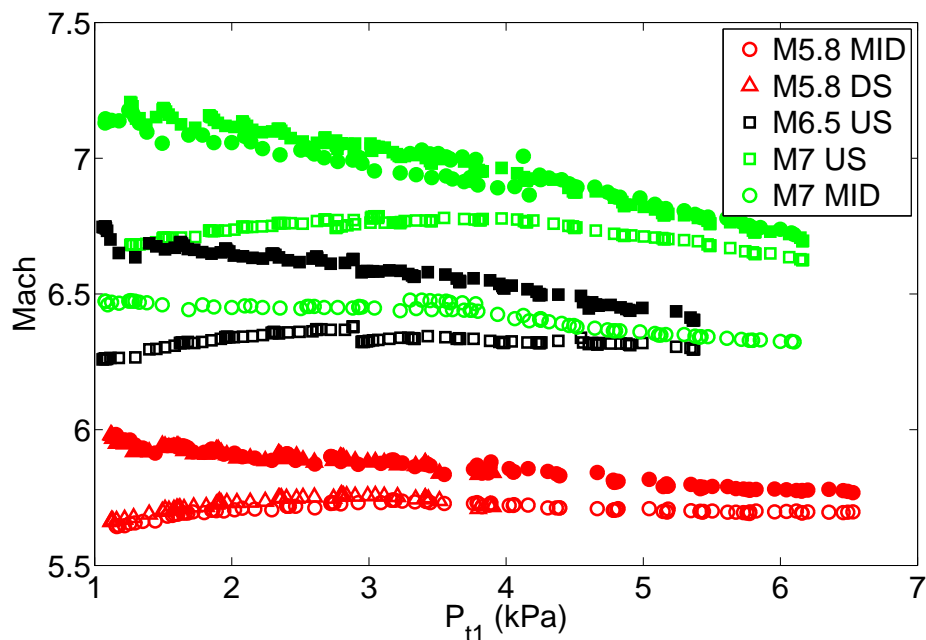


Figure 3: Mach number for all conditions. Open symbols are calculated from Pitot pressure. Closed symbols are from P_{t1} and P_1 .

For the Mach 5.8 condition, the Mach number determined from the Pitot sensor matches at both the MID and DS stations. However, the indicated Mach number is considerably lower than the desired Mach 5.8. For the Mach 6.5 condition, the Mach number as determined from the Pitot sensor is also lower than expected. The Mach 7 condition at the US station likewise shows a lower Pitot Mach number. At the MID location for the Mach 7 condition, the Pitot-indicated Mach number drops still further to about 6.5. In all instances, the Mach number as determined from P_{t1} and P_1 is higher than that determined from P_{t1} and P_{t2} and is close to the desired Mach condition.

The discrepancy in the Pitot-indicated Mach number appears to stem from an issue with the calibration of the Pitot sensor. The Pitot was calibrated with a Baratron pressure transducer at actual flow conditions ($(M=5.8, T_0=430K)$, $(M=6.5, T_0=460K)$, $(M=7, T_0=460K)$). It is found that both the sensitivity and 0-intercept change with each condition. This also holds true when the Mach 5.8 stagnation temperature is increased to 460K, indicating that the changing calibration is not just an effect of the temperature. The calibration appears to be Mach-number dependent. This result is unexpected and cannot be explained at present. When the on-condition Pitot calibration is used to calculate Mach number, a lower-than-expected Mach is indicated. Thus, the Mach number as indicated by P_{t1} and P_1 is taken to be the actual flow Mach number. When freestream Pitot disturbances are presented, they are normalized by the mean measured P_{t2} . Thus, any effect of sensor sensitivity is removed.

Figure 4 shows the P_{t2} RMS pressure normalized by P_{t2} as a function of Reynolds number for all Mach number and stations that were tested. For all conditions, the RMS fluctuations are below about 1% for $Re < 3 \times 10^6/m$. For increasing Reynolds numbers, the RMS quickly increases, peaking between 2–2.75% for Reynolds numbers from $4-5 \times 10^6/m$. Increasing Mach number appears to slightly delay the rapid increase in noise. The dramatic increase in noise is attributed to one or more of the nozzle wall boundary layers suddenly transitioning from laminar to turbulent. This hypothesis has not yet been proven, but will be the subject of future experiments. When phenomenon are measured on the model, the rapidly changing nature of the freestream disturbance field must be a consideration.

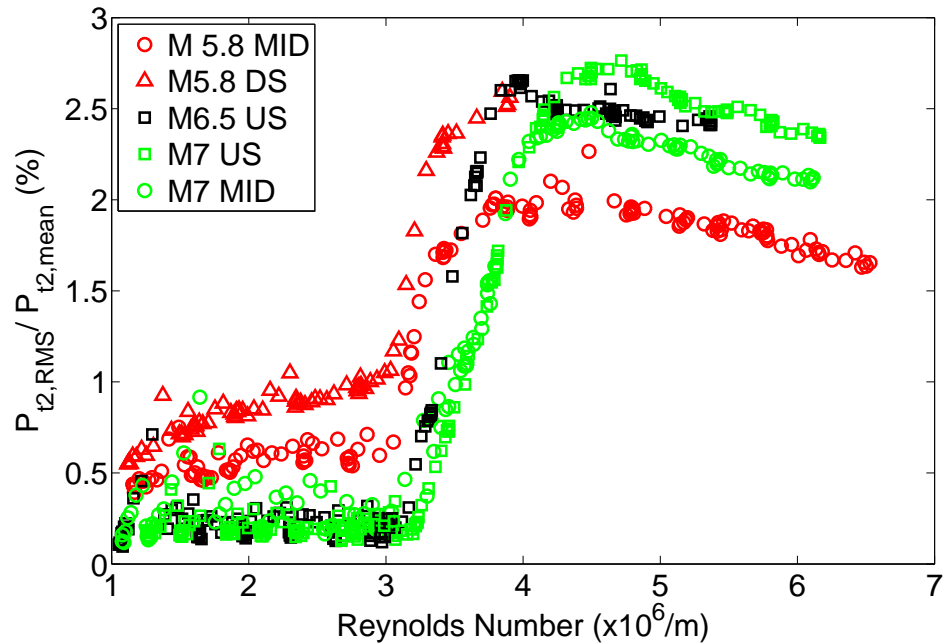


Figure 4: Freestream Pitot RMS

IV. Mach 5.8

IV.A. ACE Experiments

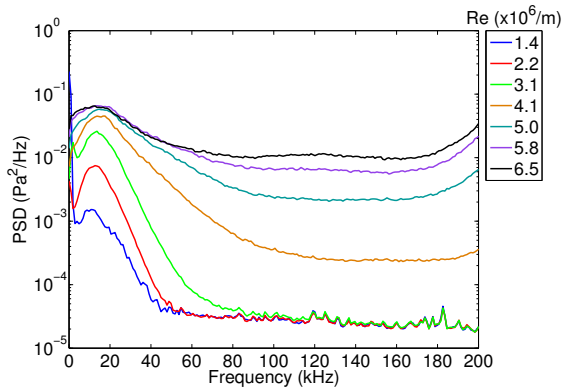
For the Mach-5.8 condition, a full freestream Reynolds number sweep was performed at the MID location. Only the lower half of the Reynolds number sweep was completed at the DS location. For higher Reynolds numbers, the tunnel would not start properly.

Figure 5 shows power spectral densities (PSDs) for model sensor 5 for $Re=1.5\text{--}6.5\times 10^6/m$. Dimensional spectra are shown, as well as spectra normalized by the tunnel stagnation pressure and the freestream RMS Pitot pressure. Figure 5d shows the corresponding PSDs of the Pitot probe signal normalized by the total pressure at similar freestream conditions.

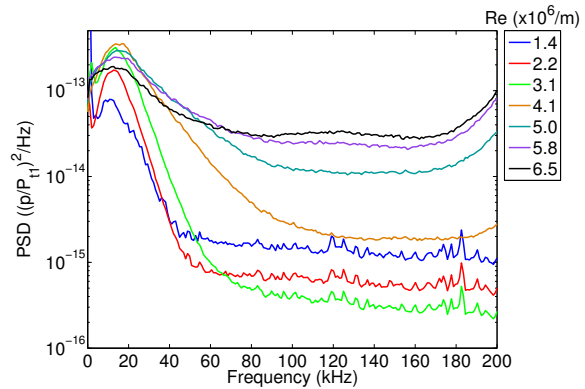
A peak in the spectra near 15 kHz is observed for the model sensor. The Pitot spectra do not show any distinct peak for these frequencies. The peak frequency increases slightly from 13–18 kHz with increasing Re for $Re=1.5\text{--}4.1\times 10^6/m$. For larger Re , the peak frequency remains invariant. This corresponds to the Reynolds number range with elevated freestream noise as seen in Figure 4. The PSDs for the model sensor normalized by the total pressure (Figure 5b) demonstrate that the amplitude of the disturbance increases in amplitude relative to the increased total pressure for $Re=1.5\text{--}4.1\times 10^6/m$. When the model sensor signal is normalized by the freestream RMS Pitot pressure, growth of the disturbance is observed again for $Re=1.5\text{--}3.1\times 10^6/m$. The amplitudes for larger Re collapse. A significant broadband power increase also occurs between $Re=3.1$ and $4.1\times 10^6/m$. It appears that the disturbance grows relative to the freestream conditions for $Re=1.5\text{--}3.1\times 10^6/m$, but then at larger Re scales with the freestream conditions.

The BAM6QT experiments with quiet flow measured traveling crossflow waves with peaks between 45 and 50 kHz for freestream Reynolds numbers of $8\times 10^6/m$.^{18,19} No similar peaks are evident in the ACE data, even for the lower-noise freestream from $Re=1\text{--}3\times 10^6/m$. However, the lowest Reynolds number for which the traveling crossflow instability was detected in the quiet flow of the BAM6QT was about $6\times 10^6/m$.

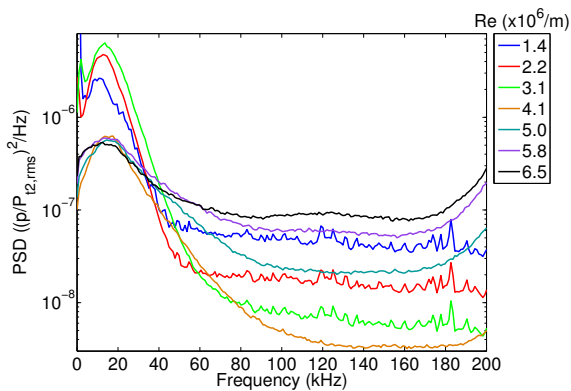
Of additional interest is the spectra from the Pitot sensors (Figure 5d). A narrow peak is observed at about 9 kHz for the lower Reynolds numbers. It is thought that this prominent disturbance may be due to a resonance in the settling chamber or an effect of the flow-conditioning screens. The spectra from the model sensor at the MID location for $Re=1.4\times 10^6/m$ also shows a small peak at this frequency. Beyond this small effect, the 9 kHz freestream disturbance does not appear to influence the model boundary layer. Experiments are planned to determine the nature and cause of this disturbance. The 15 kHz disturbance



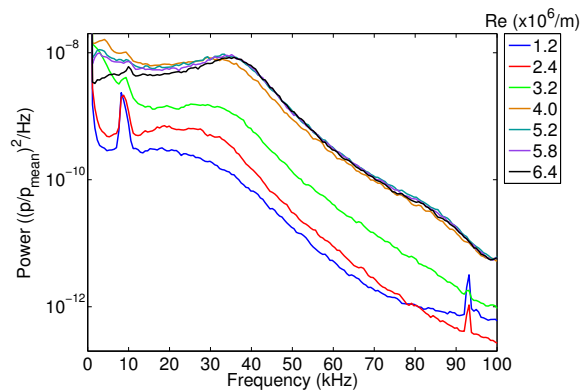
(a) Dimensional PSDs for model sensor 5



(b) PSDs for model sensor 5 normalized by freestream total pressure



(c) PSDs for model sensor 5 normalized by freestream Pitot RMS



(d) PSDs for Pitot sensor normalized by P_{t2}

Figure 5: Dimensional and normalized PSDs for model sensor and freestream Pitot at MID station, Mach 5.8

observed on the model is not correlated to any feature of the Pitot spectra.

Figure 6 shows dimensional and normalized spectra for model sensor 5 and the freestream Pitot probe at the DS station. Figure 6c, which shows spectra for the sensor signal normalized by the freestream RMS Pitot pressure, does not include spectra for all of the Reynolds numbers because the tunnel run employing the Pitot sensor was not able to capture the entire Reynolds number range as the run with the model in the tunnel. A low frequency peak centered around 14 kHz is observed for Reynolds numbers greater than $0.8 \times 10^6/m$. Again, this low-frequency peak is not correlated with any feature of the Pitot spectra. There is no change in the peak frequency with increasing Re. When the model sensor is normalized by the freestream total pressure (Figure 6b), the peak amplitude collapses for $Re=2.4-4.4 \times 10^6/m$. When the model sensor is instead normalized by the RMS Pitot pressure (Figure 6c), the peak amplitude collapses for $Re=1.7-2.8 \times 10^6/m$. It appears that the 14 kHz disturbance grows slightly relative to the freestream conditions for low Re. Over most of the Reynolds number range tested, however, it seems to scale with the freestream conditions.

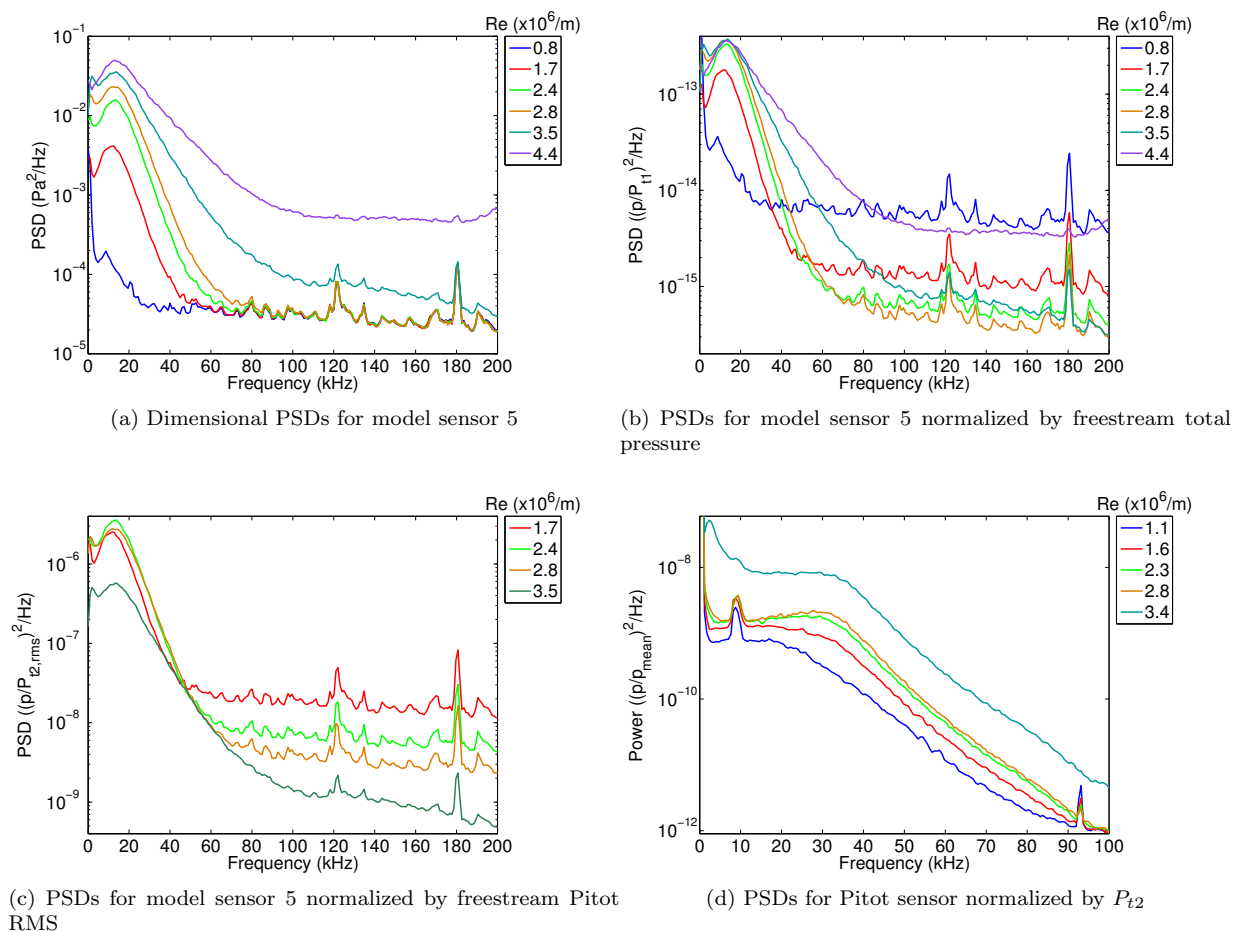


Figure 6: Dimensional and normalized PSDs for model sensor and freestream Pitot at DS station, Mach 5.8

The coherence for model sensor-pair 1-5, wave angle, and phase velocity of the low-frequency disturbances between 14 and 18 kHz are shown in Figure 7 for MID and DS stations at all the Reynolds numbers shown in Figures 5 and 6. Sensors 1, 3, and 5 are used to calculate the disturbance properties because the coherence values among these three sensors is typically the highest of the 10 possible sensor pairs. The inclusion of sensors displaced farther in span resulted in significantly reduced coherence. A similar drop in spanwise coherence was observed for the second mode on a sharp cone.³⁰ The frequency range for the wave angle and phase speed plots corresponds to frequencies for which the coherence for both sensor pairs is greater than about 0.1. For lower coherence, there is little correlated signal among all three sensors, and disturbance properties would be meaningless. At the DS station for $Re=0.8 \times 10^6/m$, disturbance properties are not

shown. At this condition, the coherence of the disturbance proved too low. The resultant wave-angle- and phase speed-spectra were too erratic to be useful.

The coherence at the peak frequency for model sensor-pair 1-5 at the MID station increases slightly between $Re=1.4$ and $2.2 \times 10^6/m$. Further increases in Re serve to decrease the coherence. This is likely due to the transitioning boundary layer. As the boundary layer moves toward a fully turbulent state, correlated disturbances are lost in the turbulence. Additionally, the frequency range for which the coherence is greater than 0.1 narrows with increasing Re . For frequencies greater than 60 kHz, the coherence is never greater than 0.1, indicating little correlation between disturbances at those frequencies between the two sensor locations. Similar behavior is seen for the coherence at the DS station. However, the coherence values do not drop as low since the Reynolds number was never large enough to cause a fully turbulent boundary layer on the model.

At the MID station, the disturbance wave angles are very similar for all Reynolds numbers. Near the 13–18 kHz peak, the average wave angle is approximately 70° . The phase speeds at the MID station are not in as good agreement as the wave angles, but are still reasonably close. It appears that as Re increases, the disturbance properties begin to depart from what is observed for lower Re . At the MID station, the average phase speed near the spectral peak is about 235 m/s.

At the DS station, the general trend of the disturbance properties are similar to what is observed at the MID station. However, the average wave angle and phase speed at the 18 kHz spectral peak are approximately 67° and 290 m/s, respectively. The cause of the change in the phase speed between the MID and DS stations is unknown. The Pitot-indicated Mach number between the two stations was within 0.5%. The stagnation temperatures were similar for the MID and DS runs. The DS station does have considerably higher Pitot fluctuations, but it is unclear how elevated freestream noise could impact the phase speed of the disturbance.

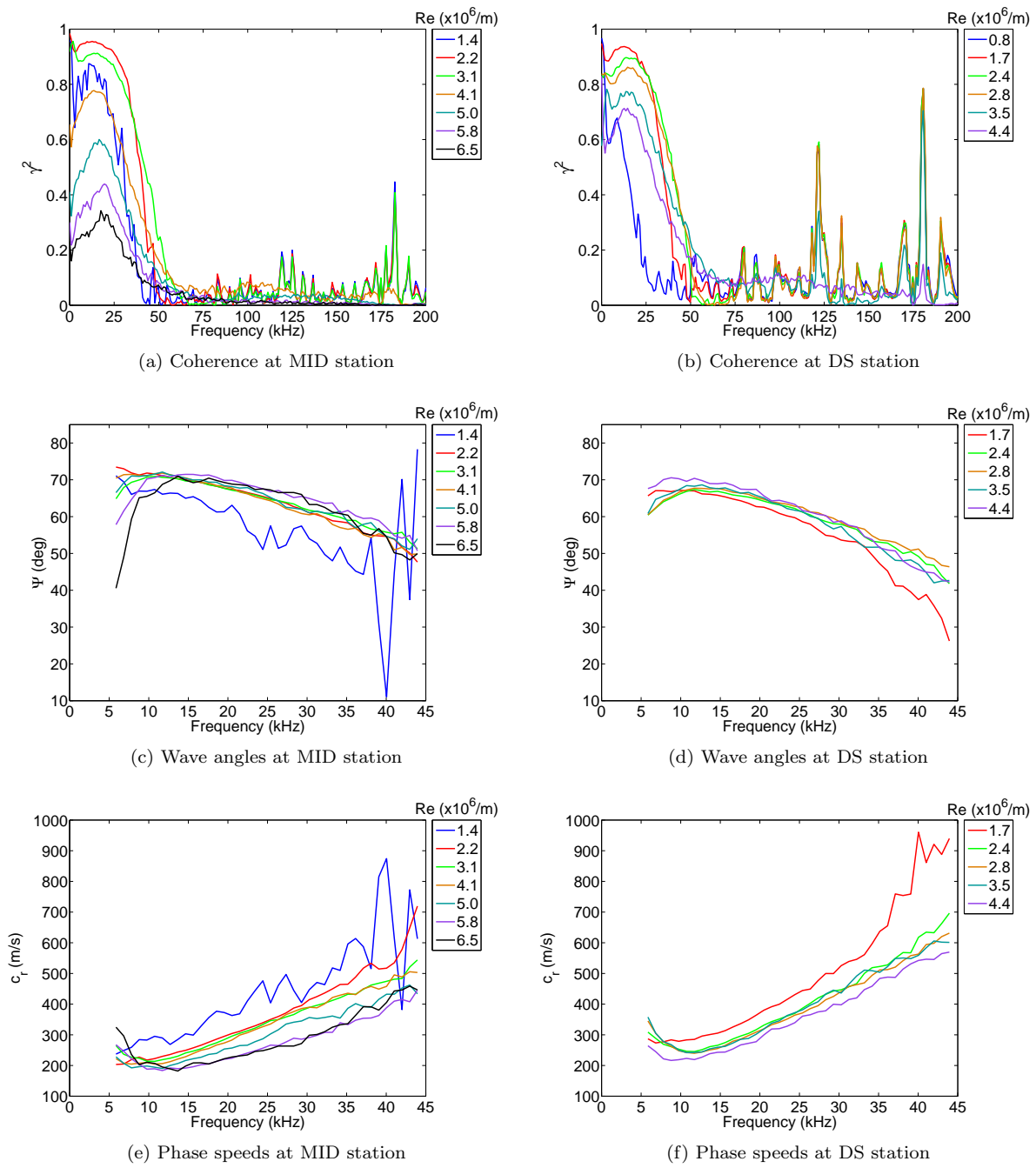


Figure 7: Coherence, wave angle, and phase speed for disturbances for Mach 5.8 at MID station

Downloaded by AFRL D'Azzo Wright-Patterson on June 17, 2015 | http://arc.aiaa.org | DOI: 10.2514/6.2015-0278

IV.B. Tunnel Comparison

IV.B.1. Disturbance Properties

Of great interest is how the model boundary layer behaves in the ACE as compared to the BAM6QT. Figure 8a shows spectra for model sensor 3 in both tunnels. For the ACE spectra, the Mach number was 5.8 and the model was at the MID streamwise station. For the BAM6QT spectra, the tunnel was run noisy and the Mach number was approximately 5.8. For each freestream Reynolds number shown, overall power levels were always significantly higher in the BAM6QT than in ACE. The 15 kHz disturbance observed in ACE is not as evident in the BAM6QT data.

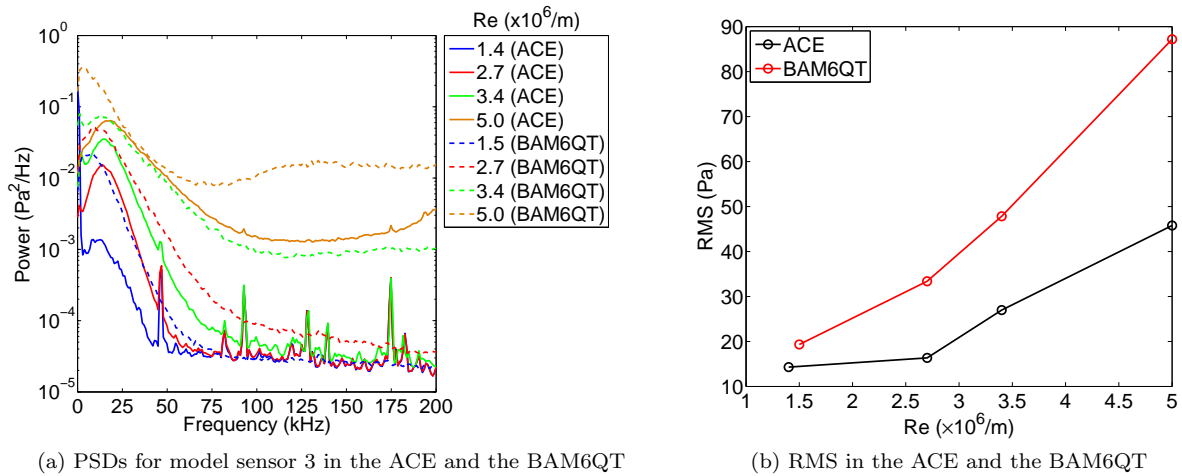


Figure 8: Mach 5.8, PSDs and RMS for model sensor 3 in the ACE and the BAM6QT

Figure 8b shows the RMS from 0–200 kHz for both tunnels. As Re increases, the RMS in the BAM6QT becomes increasingly greater than in the ACE. It is suspected that this behavior is a function of the freestream disturbance environment. Although no freestream Pitot measurements exist for the BAM6QT at these conditions, the BAM6QT generally has normalized freestream noise levels of about 3% when run noisy.³¹ This is considerably higher than even the highest noise levels observed in the ACE (see Figure 4). It is thought that the higher noise in the BAM6QT induced earlier transition than in the ACE, even though both were run as conventional tunnels. Thus, for the same Reynolds number, the boundary layer was further along in the transition process in the BAM6QT than in the ACE.

Figure 9 shows disturbance wave angles and phase velocities for the low-frequency disturbances in both the ACE and the BAM6QT. Although the wave angles are all a few degrees lower in the BAM6QT than in ACE, the agreement is quite good. The agreement in phase velocity, especially near the 12–15 kHz spectral peak, is also good. The source of the low-frequency disturbances remains unknown, but it appears that the same disturbances are present in both wind tunnels, despite their different sizes and noise levels.

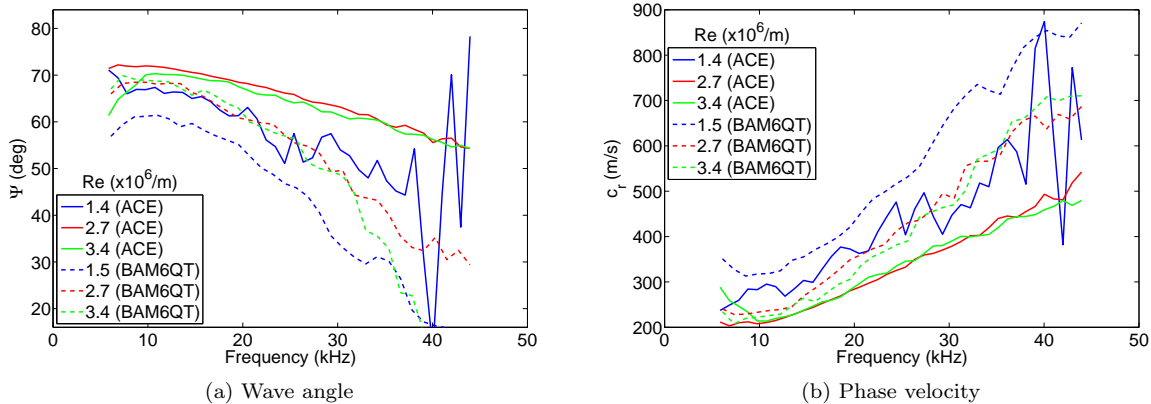
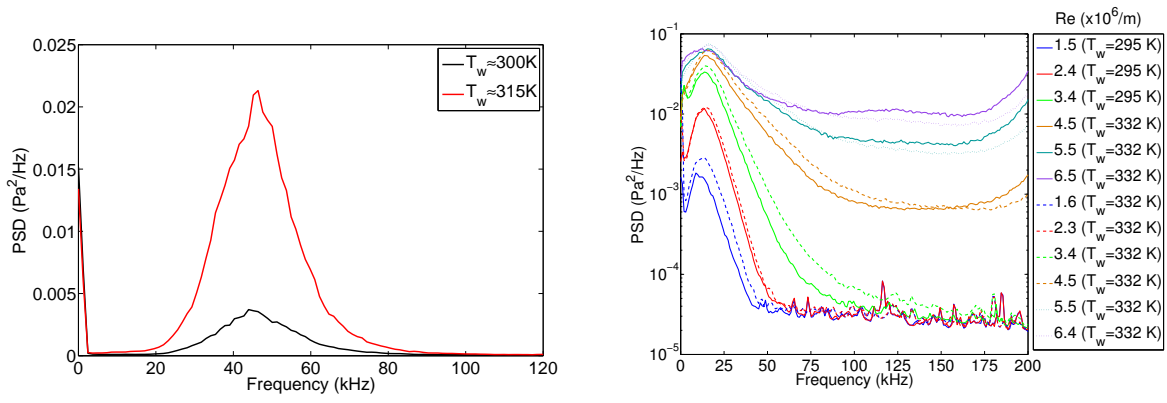


Figure 9: Wave angles and phase velocities of low-frequency disturbances in the ACE and the BAM6QT

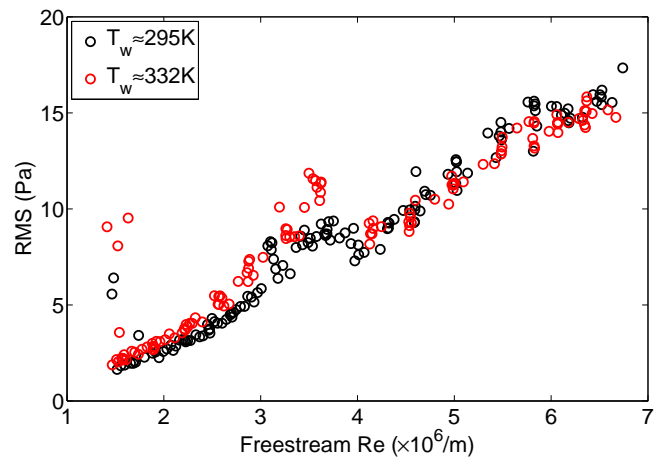
IV.B.2. Elevated Surface Temperature

The previous work in the BAM6QT raised a question that has not yet been answered. Nominally identical freestream conditions were repeated for 8 different runs over the course of one day. The freestream Reynolds number was $8.1 \times 10^6/\text{m}$ and the tunnel was run quiet. The spectra of the model sensor increased in amplitude throughout the course of the day, with the peak value being almost a factor of 5 higher during the last run of the day than during the first run of the day. This corresponds to an integrated RMS amplitude growth of a factor of about 2.2. Figure 10a shows spectra from the first and last runs of the day. The cause of this significant amplitude change was thought to be due to the model surface temperature gradually increasing throughout the course of the day, destabilizing the traveling crossflow instability. It is estimated that the model temperature increased from about 300–315 K between the first and last runs.

In order to see if a similar effect would be present for the low-frequency disturbances observed in the ACE tunnel, a series of experiments were completed with an elevated model temperature. In the case of the elevated model temperature, the model was left in the tunnel for the pre-heat portion of the run. This increased the model temperature to approximately 332 K, about 37 K higher than the baseline model temperature. Figure 10b shows spectra of model sensor 5 at five different freestream Reynolds numbers for model temperatures of 295 and 332 K. Although the amplitudes of the spectra increase, the effect is not nearly as pronounced as in the BAM6QT. Here, the maximum increase in the spectral amplitude for any Reynolds number is about 25%. Figure 10c shows the RMS amplitude from 0–50 kHz for both model temperature conditions. The elevated wall temperature is seen to slightly increase the RMS for Reynolds numbers less than approximately $3 \times 10^6/\text{m}$. For higher Reynolds numbers, the RMS is the same. This demonstrates that the low-frequency pressure fluctuations are largely insensitive to wall temperature. This result is another distinction between these disturbances and the traveling crossflow disturbances.



(a) PSD for model sensor in BAM6QT, quiet flow, (b) PSD for model sensor in ACE, Mach 5.8, MID station $Re=8.1 \times 10^6/m$



(c) RMS for model sensor in ACE, Mach 5.8, MID station

Figure 10: PSDs and RMS for model sensor 5 at varied model temperatures in the BAM6QT and ACE

IV.C. Mach 5.8 Conclusions

The nature of the low-frequency disturbances at both the MID and DS stations is unclear. The pressure fluctuations for the model sensor are dominated by the low-frequency peak in the spectra. This peak is not correlated with any feature in the Pitot spectra. At the MID station, both the amplitude and frequency exhibit modest growth up to $Re=4.1\times 10^6/m$. The amplitude grows in excess of the increasing freestream pressure. These behaviors may suggest a slowly-growing instability. At the MID station, for $Re=3.1-4.1\times 10^6/m$, the spectrum begins to fill in at higher frequencies. This is the same Re range for which the freestream RMS Pitot pressure increases substantially. Above this Reynolds number, the amplitude of the peak in the spectrum scales with the RMS Pitot pressure. This behavior implies that the model disturbances are either driven by the freestream fluctuations or that they grow with the Reynolds number in the same way that the Pitot fluctuations do.

For frequencies between 10 and 40 kHz, the model disturbances show coherence values greater than 0.1, and well-defined phase speeds and wave angles. There is little variation of wave properties with Reynolds number. The wave angle and phase speed for a frequency near the spectral peak is very similar to what was measured in the quiet flow of the BAM6QT at $Re=8.1\times 10^6/m$.¹⁸ However, the frequency is much lower than the 45-50 kHz observed in those experiments, even though the Reynolds number is 20–80% of the quiet tunnel value. Similar observations can be made at the DS station. However, at the DS station, the peak frequency does not seem to change with Re and the amplitude of the spectral peak scales well with the freestream total pressure for Reynolds numbers greater than $2.4\times 10^6/m$.

Under noisy conditions in both tunnels, the surface pressure spectra are dominated by low-frequency disturbances. The structure of these disturbances (phase velocity and wave angle) is similar in both wind tunnels. Coherence measurements in the ACE show that these disturbances remain relatively well-ordered until they begin to break down into turbulence. Even after they begin to break down, these disturbances retain a similar structure, in terms of phase velocity and wave angle. This behavior, along with the slow growth of the disturbances prior to transition, is suggestive of a disturbance that is driven by the freestream noise. This behavior is markedly different from the second-mode-dominated transition for cones at zero-degree angle-of-attack. The addition of freestream noise to these flowfields merely results in larger-amplitude disturbances, including second-mode disturbances.³² The presence of large freestream disturbances appears to create a different path to transition on the elliptic cone, compared to low-disturbance levels. There is no evidence of the traveling crossflow instability in either tunnel when run noisy, even though it is evident in the quiet flow of the BAM6QT.

V. Mach 6.5

The Mach number was changed to 6.5. Experiments were only completed at the US station for this Mach number. This was the last experiment for the tunnel entry, and time did not permit testing at the MID or DS stations. Figure 11 shows PSDs for model sensor 5 as well as corresponding freestream Pitot spectra. At Mach 6.5, the low frequency peak seen at Mach 6 is not present for low Re . For Reynolds numbers greater than $3.9\times 10^6/m$, there may be a small peak, but it is much less pronounced than at Mach 5.8. In contrast to the Mach 5.8 experiments, a high frequency peak is present for Reynolds numbers ranging from $3.7-4.8\times 10^6/m$. This Reynolds number range corresponds to the sharp increase in freestream Pitot RMS pressure as shown in Figure 4. The peak frequency displays a dependence on Reynolds number, increasing from 105 to 135 kHz as Re increases from 3.7 to $4.8\times 10^6/m$. Normalizing the model sensor signal by either the total pressure or the freestream RMS Pitot pressure demonstrates that the disturbance grows with respect to the freestream conditions.

The Pitot sensor has a 140 kHz resonance. The Pitot sensor was also anti-alias low-pass-filtered at 100 kHz. As such, no freestream information is available at the peak disturbance frequency. However, the lower-frequency tail of the disturbance peak falls within the upper frequency bounds of the Pitot spectra. There are no features present in the Pitot spectra between 80 and 100 kHz that suggest that the disturbance measured on the model is correlated to a freestream feature. Of additional note are the sharp, 5 kHz and harmonic peaks in the Pitot spectra for $Re=1.1-3.2\times 10^6/m$. These are again attributed to either a resonance in the settling chamber or an effect of the flow-conditioning screens. There are no features in the spectra from the model sensor that correlate with these freestream disturbances.

Figure 12 shows the coherence for sensor pair 1-5 (the lowest coherence among the sensors used to calculate the wave angle and phase speed), as well as wave angles and phase velocities for the high-frequency

Approved for public release; distribution unlimited.

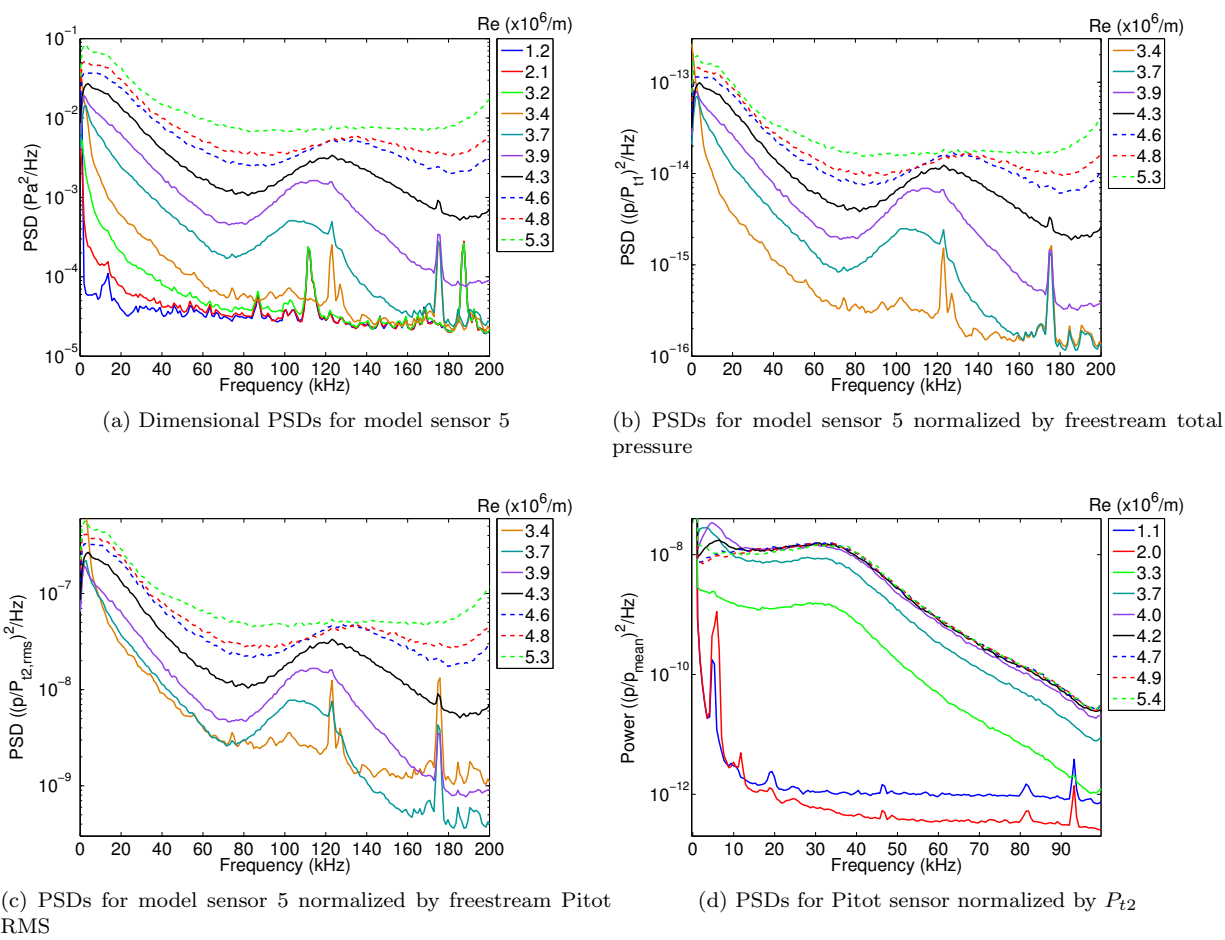


Figure 11: Dimensional and normalized PSDs for model sensor and freestream Pitot at US station, Mach 6.5

disturbances. Wave angles and phase velocities are not shown over the entire frequency domain. Rather, they are displayed only for those frequency ranges that contain the peaks in coherence. Since the peak frequency of the disturbance increases with Re , the range of frequencies for which the wave angle and phase speeds are shown also changes with Re . As Re increases and the boundary layer begins to break down, the coherence for the disturbance decreases as expected.

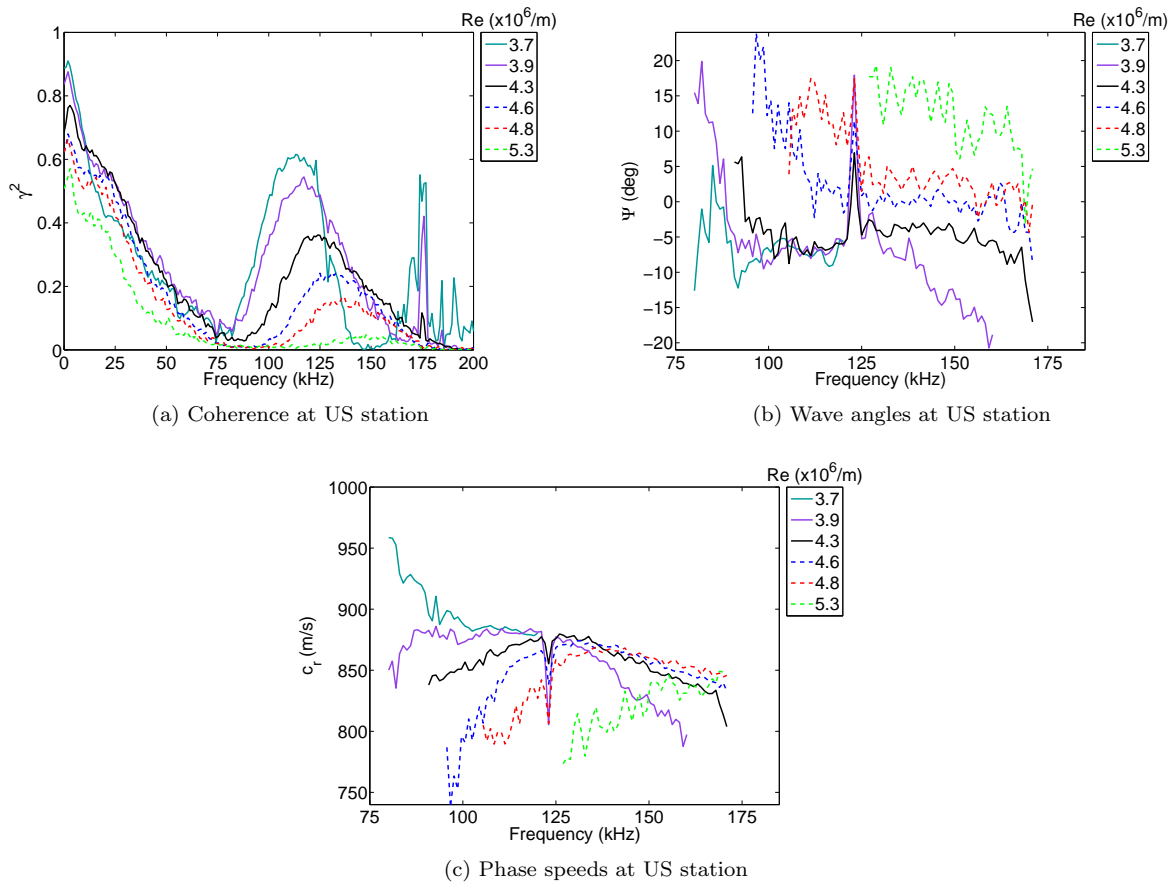


Figure 12: Coherence, wave angle, and phase speed for disturbances for Mach 6.5 at US station

The wave angles are typically shallow, ranging from -10 – 5° for the peak frequency. The phase speeds for the peak frequency are typically between 850 and 875 m/s. At Mach 6, the edge velocity at the sensor locations is 831 m/s. Thus, the high-frequency disturbances have phase speeds on the order of the expected edge velocity. The nearly 2D nature of these disturbances and phase velocity near the edge velocity may suggest a second mode instability. Computations at Mach 6 and $Re=8.1 \times 10^6/m$ predicted a second-mode frequency of 225 kHz at the sensor location.³³ Scaling this frequency by $M^2/Re^{1/2}$ to account for the thickening of the boundary layer due to the increased Mach number and decreased Reynolds number yields a frequency of 133 kHz for $Re=3.9 \times 10^6/m$ at Mach 6.5. This frequency is only 21% higher than the measured peak frequency of 110 kHz. Although this scaled frequency is not too different that what was measured, it is unclear if the second mode will scale in this manner for the elliptic cone. It is hoped that ongoing stability computations will establish the expected most-unstable second-mode frequency for these conditions, and help determine the nature of these disturbances.

VI. Mach 7

VI.A. US Station

The Mach number was increased to 7, and Reynolds number sweeps were completed at both the US and MID streamwise stations. Similar to the Mach 6.5 US condition, a high-frequency disturbance is observed

Approved for public release; distribution unlimited.

at the US station, as shown in Figure 13. However, the frequency at Mach 7 is approximately 75–80 kHz, rather than the 105–135 kHz for Mach 6.5. When the model sensor signal is normalized by the stagnation pressure or freestream RMS Pitot pressure, the disturbance is observed to grow in excess of the freestream conditions (Figures 13b and 13c).

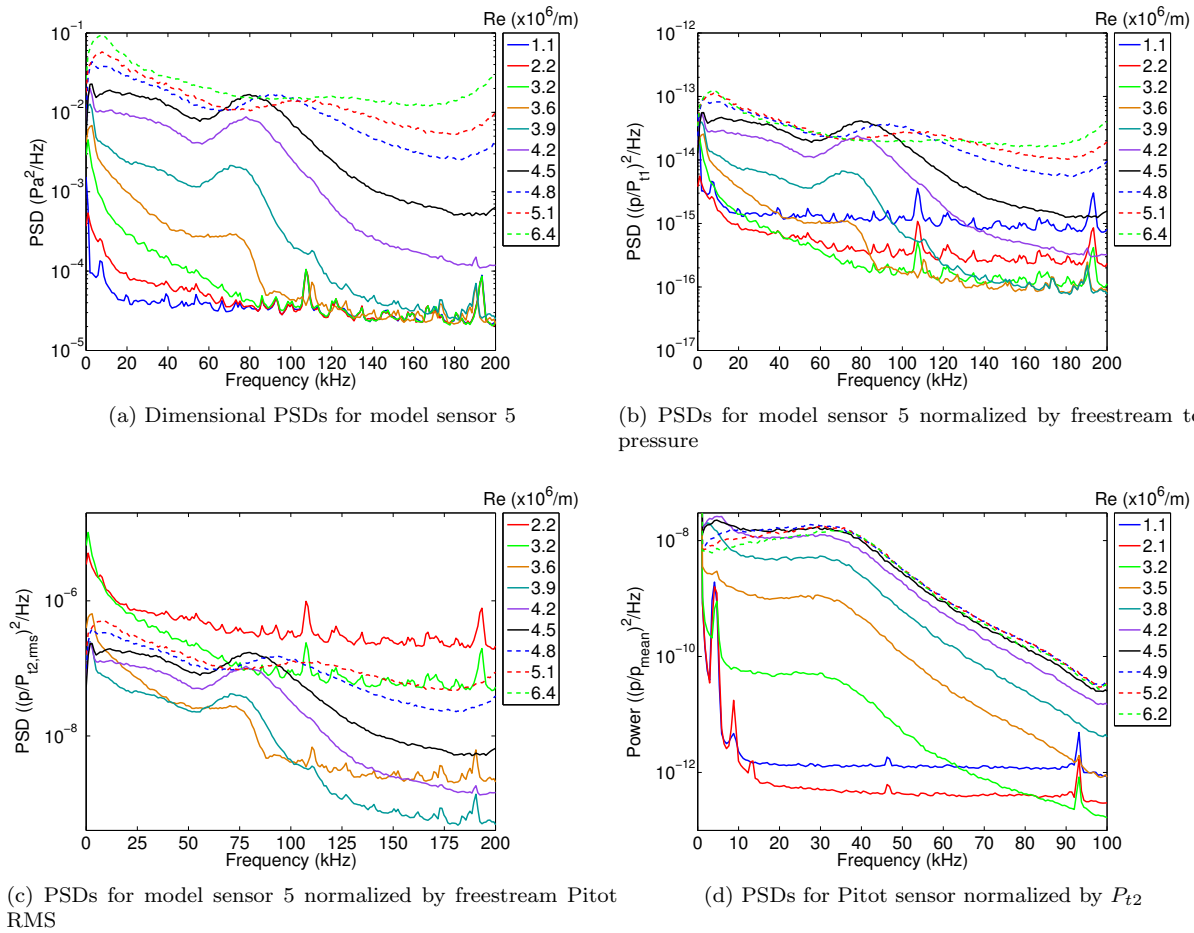


Figure 13: Dimensional and normalized PSDs for model sensor and freestream Pitot at US station, Mach 7

Narrow peaks at 4 kHz and harmonics are seen in the Pitot spectra for Re=1.1–3.5. These are again attributed to either a resonance in the settling chamber or an effect of the flow-conditioning screens. The high-frequency peaks in the model spectra are not correlated to any feature of the freestream Pitot spectra.

The coherence, wave angles, and phase speeds are shown in Figure 14. The coherence for sensor pair 1-5 shows a correlated disturbance that becomes uncorrelated as Re increases and the boundary layer transitions. For Re=6.4×10⁶/m, the coherence is near 0 for 75–200 kHz. This behavior indicates that the boundary layer is fully turbulent or nearly fully turbulent, as might also be surmised from the spectrum in Figure 13a. Disturbance properties are shown only for a subset of Reynolds numbers for which meaningful properties could be determined. Wave angles for all Reynolds numbers are again shallow, near -11° for the peak frequency. The phase velocities for all Reynolds numbers are approximately 870 m/s near the peak frequency.

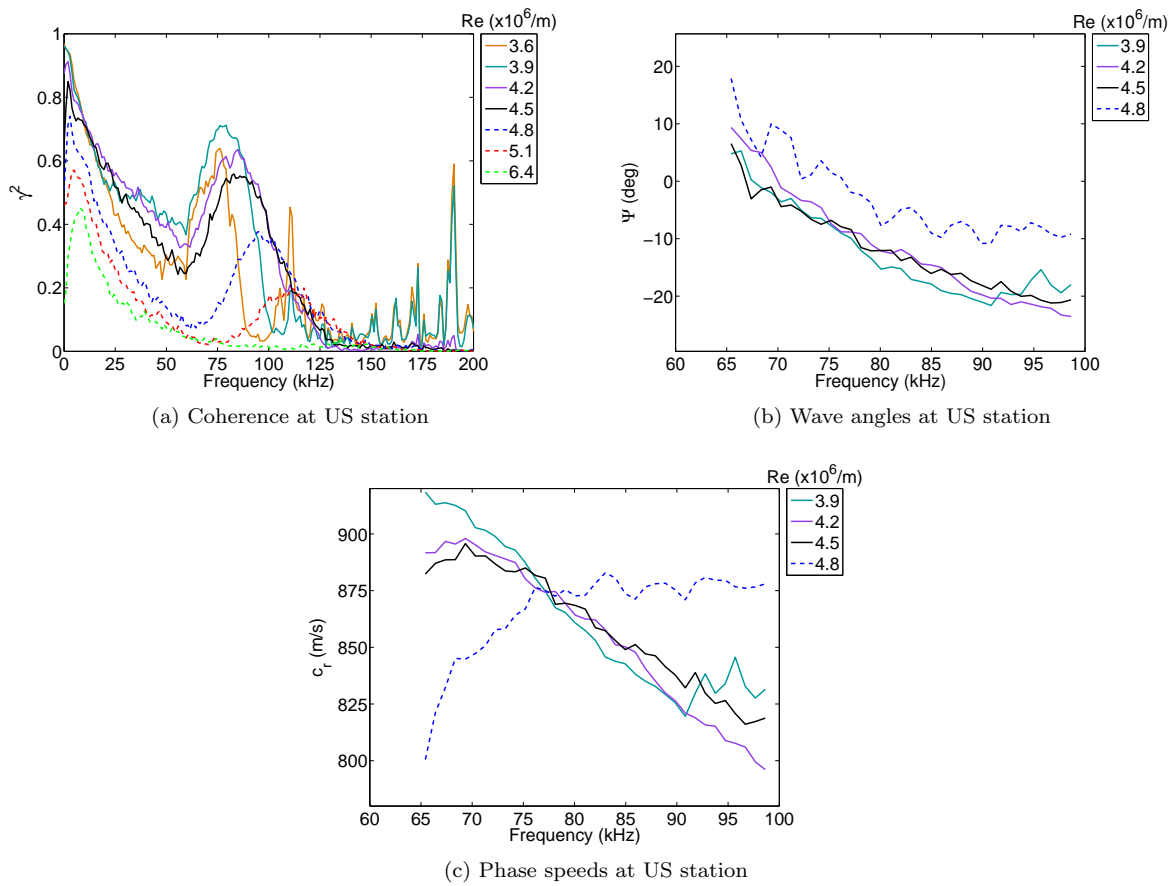


Figure 14: Coherence, wave angle, and phase speed for disturbances for Mach 7 at US station

For $Re=3.9\text{--}4.5$, the disturbance properties are nearly identical. When Re is increased to $4.8\times 10^6/m$, a departure from the lower Reynolds numbers is observed in both the wave angle and phase speed plots. This is likely due to the transitioning nature of the boundary layer. The shallow wave angles and near-edge-speed phase speeds is again suggestive of the second mode. Scaling the 225 kHz predicted second-mode frequency at Mach 6 for $Re=8.1\times 10^6/m$ by $M^2/Re^{1/2}$ gives a frequency of 115 kHz for $Re=3.9\times 10^6/m$. This frequency is within 53% of the measured 75 kHz peak frequency. Although this scaled frequency does not agree with the measured frequency as well as the Mach 6.5 case, it does demonstrate the expected trend for the second mode, even if the second mode for the elliptic cone does not scale in exactly this manner. The cause of the 80 kHz disturbance is unknown. It is again hoped that ongoing stability computations will help determine the nature of these disturbances.

VI.B. MID Station

Figure 15 shows the dimensional and normalized PSDs for model sensor 5, as well as the spectra for the Pitot probe at the MID station. When compared to the US station, several very different behaviors are observed. There is no evidence of the 80 kHz peak that was present at the US station. However, for $Re > 4.1\times 10^6/m$, a low-frequency peak at about 20 kHz is observed. Additionally, it appears that the model boundary layer remains laminar for all Reynolds numbers tested. Normalizing the model sensor's signal by the freestream total pressure or the RMS Pitot pressure collapses the spectra near 20 kHz for Reynolds numbers greater than $4.1\times 10^6/m$ (Figures 15b and 15c). The 20 kHz disturbance does not grow in excess of the increasing freestream pressure and noise. It appears that this disturbance is a response to the freestream conditions, and not a growing instability.

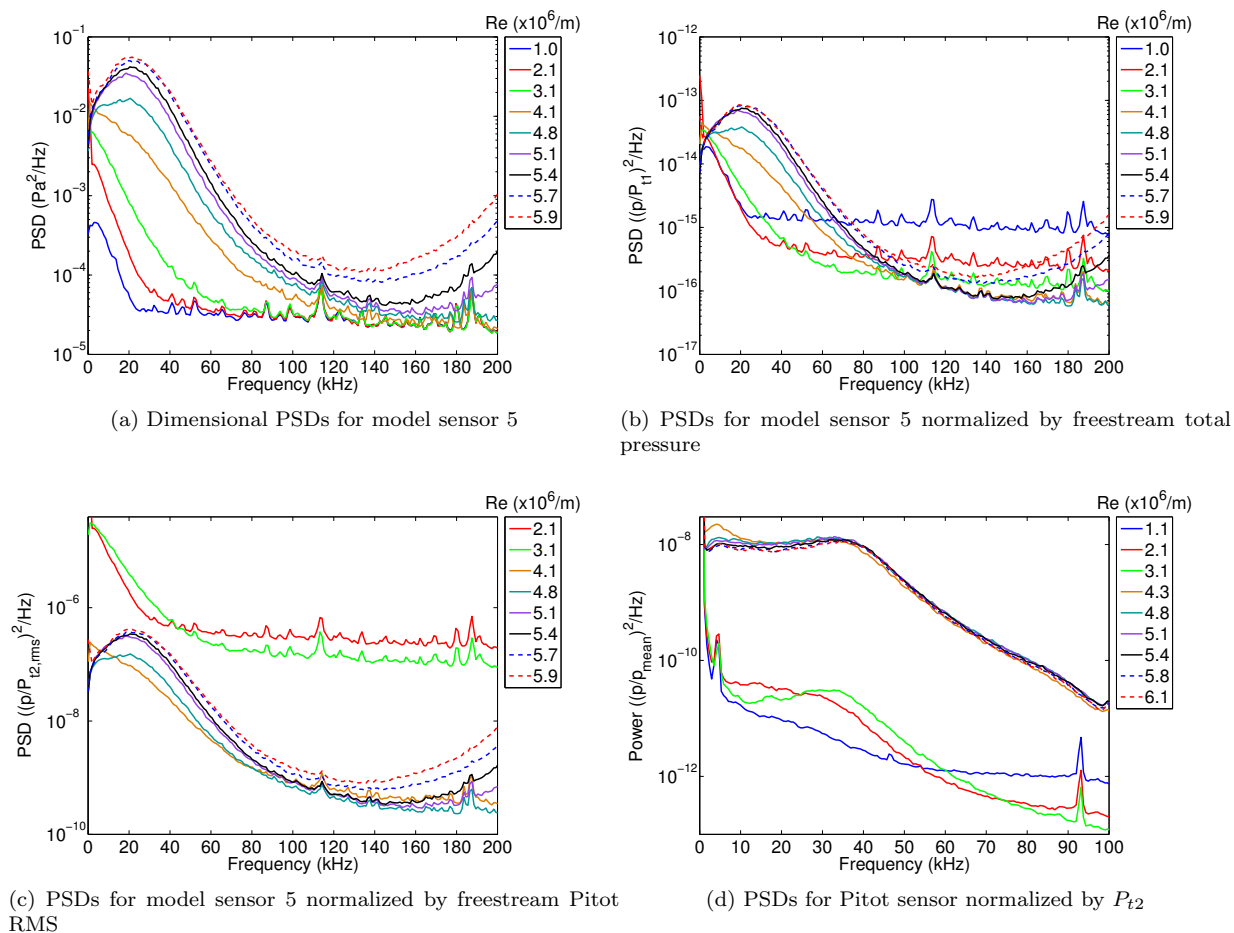


Figure 15: Dimensional and normalized PSDs for model sensor and freestream Pitot at MID station, Mach 7

7

The coherence, wave angles, and phase speeds at the MID station are shown in Figure 16. It is clear from the coherence plot that the 20 kHz disturbance begins to be correlated among the sensors for $Re=4.1 \times 10^6/m$. For larger Re , the coherence is greater and the peak is more prominent and nearly identical for all Reynolds numbers. The wave angles and phase speeds for $Re=4.8-5.9$ also exhibit good agreement, with the wave angle and phase speeds near the peak frequency being about 68° and 250 m/s, respectively. Even if this disturbance is not an instability, it shows remarkably consistent disturbance properties.

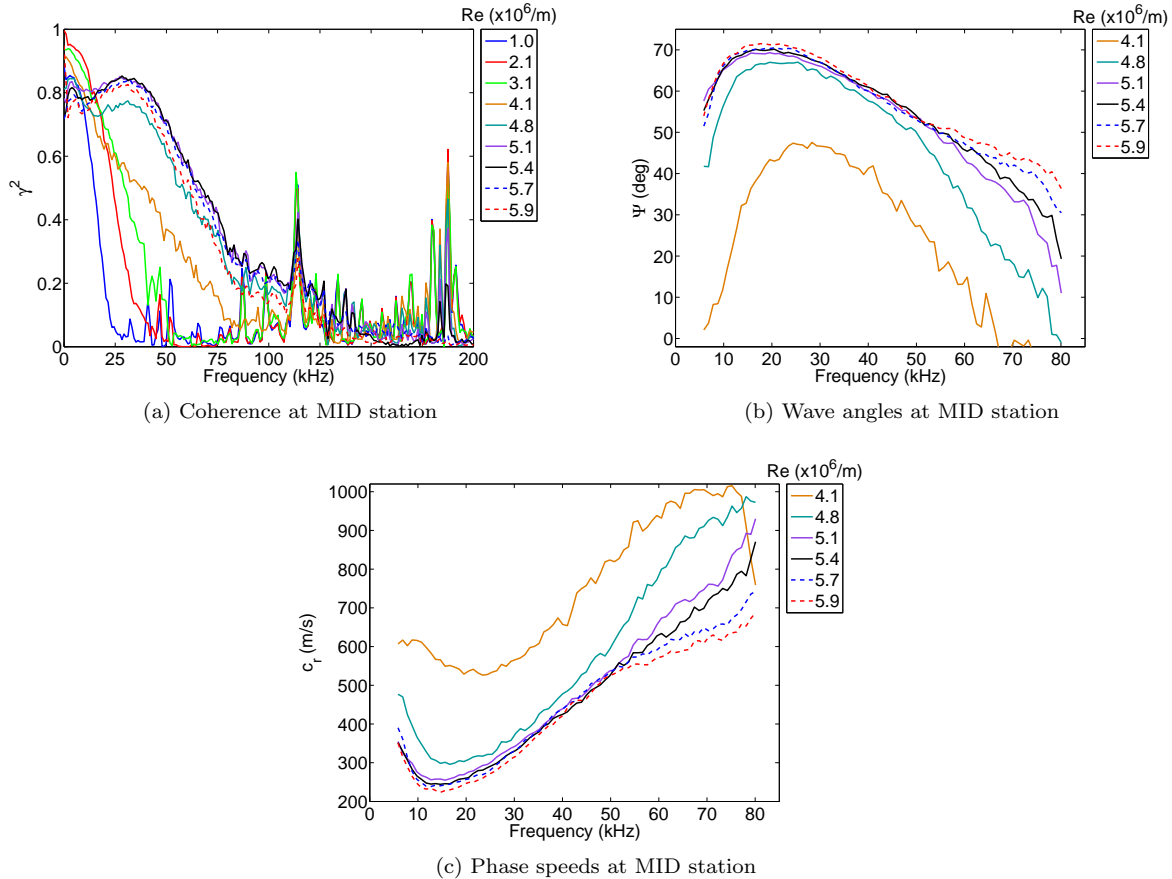


Figure 16: Coherence, wave angle, and phase speed for disturbances for Mach 7 at MID station

The cause of these very different boundary layer behaviors at Mach 7 between two streamwise stations in the tunnel is unknown. However, it seems likely that it is a function of freestream conditions changing in the streamwise direction. Figure 3 shows that the Mach number based on P_{t2} and P_{t1} is approximately 0.2 lower at the MID station than at the US station. Such a discrepancy cannot be explained by sensor calibration nor temperature effects. The actual flow conditions at the MID location are thus unknown. It is remarkable, however, that transition at the MID station is not observed, even for the highest Reynolds number.

VII. Freestream Condition Comparison

Figure 17 shows the RMS from model sensor 5 as a function of freestream Reynolds number. Here, the RMS is calculated by integrating the PSDs from 0-200 kHz. When the model is in the US station, the RMS increases almost linearly with Reynolds number for $Re=1-3 \times 10^6/m$. For higher Re , the RMS increases at a much greater rate. The change in slope corresponds to the Reynolds number for which the Pitot pressure RMS begins to rapidly increase at those stations. The high-frequency disturbances at both Mach 6.5 and 7 are first observed at $Re \approx 3.6 \times 10^6/m$.

For Mach 5.8 at the MID and DS stations, the model sensor RMS increases almost linearly with Re across the entire range of Re tested, even though the Pitot sensor RMS shows a sharp increase in RMS for

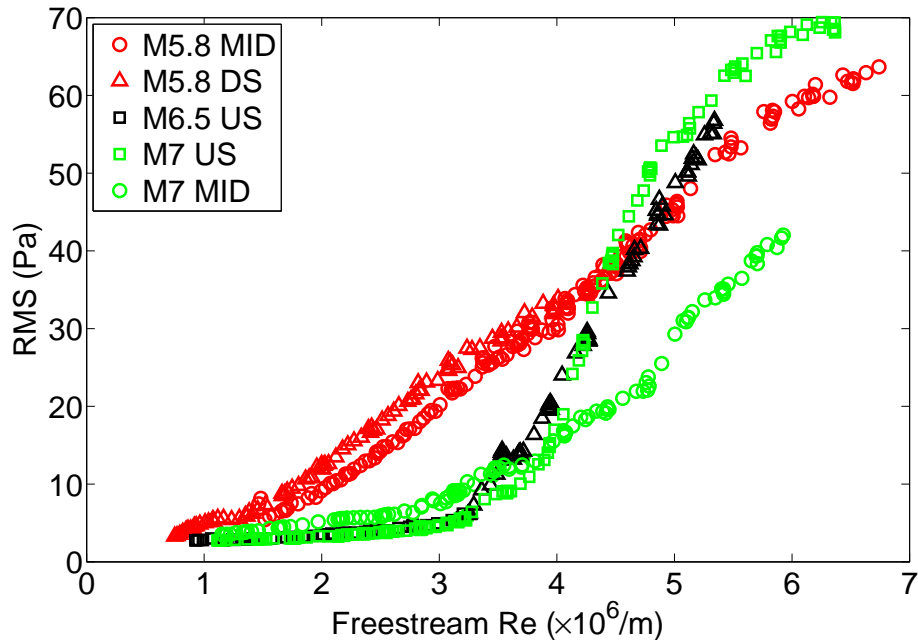


Figure 17: RMS for model sensor 5 for all freestream conditions

$Re > 3 \times 10^6/m$. The model boundary layer is observed to transition, so a sharp upturn in the RMS was also expected. It is unclear why the RMS simply increases linearly with Reynolds number.

The Mach 7 MID station RMS is markedly different than all other conditions. The RMS tracks well with the Mach 6.5 and 7 US conditions for $Re = 1-3 \times 10^6/m$. For larger Re , the Mach 7 MID case continues to increase, but not as rapidly as any of the other conditions. The Pitot RMS for Mach 7 MID also has a sharp upturn at $Re = 3 \times 10^6/m$. This behavior highlights the unknown nature of the flow at the Mach 7 MID condition.

VIII. Summary and Conclusions

A 38.1% scale model of the HIFiRE-5 elliptic cone was tested in the ACE tunnel. Freestream Reynolds number, Mach number, model position, and model temperature were all varied to look for traveling crossflow waves. Low-frequency disturbances at 12–15 kHz are observed for Mach 5.8 at the MID station. As Re increases from 1.4 to $3.2 \times 10^6/m$, the disturbance appears to grow in excess of the increasing freestream pressure and noise. For larger Re , any amplitude growth of the disturbances can be accounted for by the increasing freestream pressure and/or noise. Similar behavior is observed at the US station. It seems unlikely that this low-frequency disturbance is an instability, but it does appear to be a weak response to the changing freestream conditions. An increased model temperature has a negligible effect on the amplitudes of the low-frequency disturbances.

At Mach 6.5 and 7 at the US station, unexpected high-frequency disturbances were also measured at about 120 and 80 kHz, respectively. The wave angles were very shallow (nearly 2D waves), and the phase velocities were on the order of the edge velocity. These qualities suggest that these disturbances may be due to the second mode instability. The trend of decreasing peak frequency with increasing Mach number is expected for the second mode. Ongoing stability computations are necessary to further refine an expected second mode frequency for each condition.

A low frequency disturbance at about 20 kHz is observed at Mach 7 for the MID station. Most of the growth of this disturbance is accounted for by the increasing freestream pressure and noise. Additionally, the model boundary layer at this condition appears to never transition. Freestream properties are clearly varying in the streamwise direction. The actual flow properties at the Mach 7 MID station are unknown, but they are not sufficient to transition the model boundary layer at the sensor location, even for the highest Reynolds number tested.

Approved for public release; distribution unlimited.

Observations at the Mach 5.8 MID station in the ACE are similar to those in the BAM6QT when it is run as a conventional tunnel. For the same Reynolds number, spectra from the BAM6QT consistently show higher power levels across the frequency range. The model sensor RMS pressure in the BAM6QT is always higher when compared to the ACE. Wave angles and phase speeds for the 20 kHz disturbance are similar in both tunnels. The nature of the 20 kHz disturbance is unclear, but it appears to be related to the properties of the freestream acoustic environment in the tunnels. The traveling crossflow instability is not observed in the conventional flow of either tunnel, despite its prominence in quiet flow. This result underscores the need for caution when extrapolating transition measurements from noisy environments to quiet.

One of the objectives of this study was to provide a preliminary assessment of tunnel noise effects on HIFiRE-5, and to inform future HIFiRE-5 experiments in the TAMU tunnels. Based on the current experiments, several future experiments in the ACE tunnel are suggested. These include detailed mapping of disturbance fields in the wind tunnel, including higher-frequency measurements, multi-point probe measurements to help determine freestream disturbance structure and to begin separating fluctuation modes. Detailed mapping of the tunnel mean flow at various conditions should also be considered. Visualization of the model transition front, using infrared thermography or temperature-sensitive paint would also help to interpret results and possibly to determine if stationary crossflow vortices are also present.

References

- ¹Dolvin, D., "Hypersonic International Flight Research and Experimentation (HIFiRE) Fundamental Science and Technology Development Strategy," AIAA paper 2008-2581, April 2008.
- ²Dolvin, D., "Hypersonic International Flight Research and Experimentation Technology Development and Flight Certification Strategy," AIAA paper 2009-7228, Oct. 2009.
- ³Malik, M. R., Li, F., and Choudhari, M., "Analysis of Crossflow Transition Flight Experiment Aboard the Pegasus Launch Vehicle," AIAA paper 2007-4487, June 2007.
- ⁴Malik, M., Li, F., and Chang, C.-L., "Crossflow disturbances in three-dimensional boundary layers: nonlinear development, wave interaction and secondary instability," *Journal of Fluid Mechanics*, Vol. 268, 1994, pp. 1-36.
- ⁵Saric, W. S. and Reed, H. L., "Crossflow Instabilities- Theory & Technology," AIAA paper 2003-0771, Jan. 2003.
- ⁶Bippes, H., "Basic experiments on transition in three-dimensional boundary layers dominated by crossflow instability," *Progress in Aerospace Sciences*, Vol. 35, 1999, pp. 363-412.
- ⁷Corke, T. and Knasiak, K., "Stationary-traveling cross-flow mode interactions with periodic distributed roughness," AIAA paper 96-2016, June 1996.
- ⁸Bippes, H. and Lerche, T., "Transition Prediction in Three-Dimensional Boundary-Layer Flows Unstable to Crossflow Instability," AIAA paper 97-1906, 1997.
- ⁹White, E. B. and Saric, W. S., "Secondary instability of crossflow vortices," *Journal of Fluid Mechanics*, Vol. 525, 2005, pp. 275-308.
- ¹⁰Carpenter, M. H., Choudhari, M., Li, F., Streett, C. L., and Chang, C.-L., "Excitation of Crossflow Instabilities in a Swept Wing Boundary Layer," Paper 2010-0378, AIAA, January 2010.
- ¹¹Eppink, J. and Wlezien, R., "Observations of traveling crossflow resonant triad interactions on a swept wing," Paper 2012-2820, AIAA, June 2012.
- ¹²Saric, W. S. and Reed, H. L., "Supersonic Laminar flow control on swept wings using distributed roughness," AIAA paper 2002-0147, Jan. 2002.
- ¹³King, R., "Three-dimensional boundary-layer transition on a cone at Mach 3.5," *Experiments in Fluids*, Vol. 13, No. 4, 1992, pp. 305-314.
- ¹⁴Beeler, G. B., Wilkinson, S. P., Balakumar, P., and McDaniel, K. S., "Crossflow instability on a wedge-cone at Mach 3.5," Paper 2012-2825, AIAA, June 2012.
- ¹⁵Poggie, J., Kimmel, R. L., and Schwoerke, S. N., "Traveling Instability Waves in a Mach 8 Flow over an Elliptic Cone," *AIAA Journal*, Vol. 38, No. 2, 2000, pp. 251-258.
- ¹⁶Choudhari, M., Chang, C.-L., Jentink, T., Li, F., Berger, K., Candler, G., and Kimmel, R., "Transition Analysis for the HIFiRE-5 Vehicle," AIAA paper 2009-4056, June 2009.
- ¹⁷Swanson, E. O. and Schneider, S. P., "Boundary-layer transition on cones at angle of attack in a Mach-6 quiet tunnel," Paper 2010-1062, AIAA, January 2010.
- ¹⁸Borg, M. P., Kimmel, R. L., and Stanfield, S., "Crossflow Instability for HIFiRE-5 in a Quiet Hypersonic Wind Tunnel," Paper 2012-2821, AIAA, June 2012.
- ¹⁹Borg, M. P., Kimmel, R. L., and Stanfield, S., "Traveling Crossflow Instability for HIFiRE-5 in a Quiet Hypersonic Wind Tunnel," Paper 2013-2737, AIAA, June 2013.
- ²⁰Semper, M. T., Tichenor, N. R., Bowersox, R. D. W., Srinivasan, R., and North, S. W., "On the design and calibration of an actively controlled expansion hypersonic wind tunnel," AIAA paper 2009-0799, January 2009.
- ²¹Tichenor, N. R., Semper, M. T., Bowersox, R. D. W., Srinivasan, R., and North, S. W., "Calibration of an actively controlled expansion hypersonic wind tunnel," AIAA paper 2010-4793, July 2010.
- ²²Semper, M. T., Pruski, B. J., and Bowersox, R. D. W., "Freestream turbulence measurements in a continuously variable hypersonic wind tunnel," AIAA paper 2012-0732, January 2012.

- ²³Beresh, S. J., Henfling, J., Spillers, R., and Pruett, B., "Measurements of Fluctuating Wall Pressures Beneath a Supersonic Turbulent Boundary Layer," Paper 2010-0305, AIAA, January 2010.
- ²⁴Juliano, T. J. and Schneider, S. P., "Instability and Transition on the HIFiRE-5 in a Mach-6 Quiet Tunnel," AIAA paper 2010-5004, June 2010.
- ²⁵Borg, M. P., Kimmel, R. L., and Stanfield, S., "HIFiRE-5 Attachment-line transition in a Quiet Hypersonic Wind Tunnel," Paper 2011-3247, AIAA, June 2011.
- ²⁶Kimmel, R. L. and Poggie, J., "Transition on an Elliptic Cone at Mach 8," American Society of Mechanical Engineers ASME FEDSM97-3111, June 1997.
- ²⁷Kimmel, R. L. and Poggie, J. J., "Three-Dimensional Hypersonic Boundary Layer Stability and Transition," WL-TR-97-3111, Air Force Research Laboratory Technical Report, Wright-Patterson Air Force Base, Ohio, Dec. 1997.
- ²⁸Kimmel, R. L., Poggie, J. J., and Schwoerke, S. N., "Laminar-Turbulent Transition in a Mach 8 Elliptic Cone Flow," *AIAA Journal*, Vol. 37, No. 9, September 1999, pp. 1080-1087.
- ²⁹Bendat, J. and Piersol, A., *Engineering Applications of Correlation and Spectral Analysis*, Wiley-Interscience, 1980.
- ³⁰Kimmel, R. L., Demetriades, A., and Donaldson, J. C., "Space-Time Correlation Measurements in a Hypersonic Transitional Boundary Layer," *AIAA Journal*, Vol. 34, No. 12, December 1996, pp. 2484-2489.
- ³¹Chynoweth, B. C., Ward, C. A. C., Greenwood, R. T., McKiernan, G. R., Fisher, R. A., and Schneider, S. P., "Measuring Transition and Instabilities in a Mach 6 Hypersonic Quiet Wind Tunnel," AIAA paper 2014-2643, June 2014.
- ³²Estorf, M., Radespiel, R., Schneider, S. P., Johnson, H. B., and Hein, S., "Surface-pressure measurements of second-mode instability in quiet hypersonic flow," Paper 2008-1153, AIAA, January 2008.
- ³³Li, F., Choudhari, M., Chang, C.-L., White, J., Kimmel, R., Adamczak, D., Borg, M., Stanfield, S., and Smith, M., "Stability Analysis for HIFiRE Experiments," AIAA paper 2012-2961, June 2012.